

# Growth of carbon nanotubes characterized by field emission measurements during chemical vapor deposition

Jean-Marc Bonard,\* Mirko Croci,† Christian Klinke, Fabien Conus, Imad Arfaoui, Thomas Stöckli,‡ and André Chatelain  
*Faculté des Sciences de Base, Ecole Polytechnique Fédérale de Lausanne, CH-1015 Lausanne EPFL, Switzerland*

(Received 5 June 2002; revised manuscript received 2 December 2002; published 21 February 2003)

The growth of multiwall carbon nanotubes is characterized *in situ* in a chemical vapor deposition reactor by measuring the current extracted by field emission from the growing nanostructures. The lengthening of the nanotubes provokes an increase of the emitted current at constant applied voltage, and the use of a phosphor screen allows to observe the individual emitters during the growth. A simple model permits furthermore to estimate the growth rate. The nanotubes grow with a closed cap under  $10^{-2}$ – $10^{-4}$  mbar of  $C_2H_2$  at  $700^\circ C$  with a growth rate over  $1 \mu m/s$  that increases with the  $C_2H_2$  pressure. The growth of the nanotubes is neither simultaneous nor homogeneous over the cathode and involves a different activation time for every emitter.

DOI: 10.1103/PhysRevB.67.085412

PACS number(s): 81.07.De, 79.70.+q, 61.46.+w

## I. INTRODUCTION

Carbon nanotubes<sup>1,2</sup> are one of the most fascinating materials that have been discovered in recent years, since they show exceptional electronic and mechanical properties that have triggered an ever stronger effort towards applications. The possibilities are promising and range from nanotube composite materials,<sup>3,4</sup> nanoelectronics,<sup>5,6</sup> scanning microscope probes,<sup>7,8</sup> chemical<sup>9</sup> and/or biological sensors,<sup>10,11</sup> to cold electron sources.<sup>12</sup>

Nanotubes have a unique property in that their electronic behavior (semiconducting or metallic) is determined by their structure, which also determines to a great extent the overall properties of devices as wide ranging as field effect transistors, flat panel displays, or chemical sensors. This implies a precise control of nanotube diameter and chirality for molecular electronics. This control is even more acute for field-emission devices, since the emitted current is extremely sensitive to the field-enhancement factor,  $\gamma$ , which is determined directly by the diameter, length, and spacing of the emitters.<sup>12–14</sup>

The realization of reliable nanotube devices will therefore depend on a reproducible growth, e.g., by chemical vapor deposition (CVD) techniques. However, little is known about the mechanisms involved in the CVD growth in spite of their utmost importance. It would be therefore highly desirable to have methods which allow to characterize nanotubes *during* instead of *after* growth. We describe here a technique which consists of measuring the field-emission properties of the growing nanotubes. After a brief introduction to field emission in Sec. II and to CVD in Sec. III, we detail the experimental setup in Sec. IV. Section V presents and discusses the experimental results.

## II. FIELD EMISSION

Field emission is the extraction of electrons from a solid by tunneling through the surface-potential barrier under the application of a strong electric field (for reviews on field emission, see Refs. 15 and 16). The potential barrier is square when no electric field is present, and becomes triangular when a negative potential is applied to the solid with a

slope that depends on the amplitude of the local electric field  $F$  just above the surface. Tunneling through the surface barrier becomes significant for fields above  $\sim 3$  V/nm.

The Fowler-Nordheim (F-N) model of field emission dates back to the beginnings of quantum mechanics and is still widely used today.<sup>16</sup> Although this model has been originally developed for flat metallic surfaces at 0 K, it has proven adaptable to describe field emission from carbon-based electron emitters.<sup>17</sup>

The F-N model states that the current  $I$  (A) per emitter varies with the local field at the emitter surface  $F$  (V/m) as

$$I = A \frac{1.56 \times 10^{-6}}{\phi \times t(y)} F^2 \exp\left[-\frac{6.83 \times 10^9 \phi^{1.5}}{F} v(y)\right], \quad (1)$$

where  $A$  has the dimension of an area [ $m^2$ ] and represents in first approximation the emitting area,  $\phi$  is the work function in eV, and  $t(y)$  and  $v(y)$  are the Nordheim elliptic functions with  $y = \sqrt{e^3 F / 400 \pi \epsilon_0 \phi^2}$ . These functions can be approximated by  $t^2(y) \approx 1.1$  and  $v(y) \approx 0.95 - y^2$ , yielding<sup>18</sup>

$$I = A \frac{1.5 \times 10^{-6}}{\phi} F^2 \exp\left(\frac{10.4}{\sqrt{\phi}}\right) \exp\left(-\frac{6.44 \times 10^9 \phi^{1.5}}{F}\right). \quad (2)$$

Equation (2) shows that for typical values encountered in carbon-based emitters [ $A = 10^{-12}$ – $10^{-14} m^2$ ,  $\phi = 4.9 \pm 0.1$  eV (Ref. 19)] one obtains a current of  $I = 1$  nA at  $F = 3.3 \pm 0.4$  V/nm.

To reach the field of  $\sim 3$  V/nm necessary to extract electrons, one usually uses sharp objects or protusions on a surface to amplify the electric field. In that case, the local electric field is not simply  $V/d$  (applied voltage,  $V$ , divided by interelectrode distance,  $d$ ) but is higher by a factor  $\gamma$ , which gives the aptitude of the emitter to amplify the field and is accordingly termed the field-enhancement factor.  $\gamma$  is a strictly geometrical parameter that depends on the dimensions and shape of the emitter and on its surroundings, as well as on the shape and distance of the counterelectrode. The field at the emitter surface is written as  $F = \gamma V/d$ , and Eq. (2) becomes

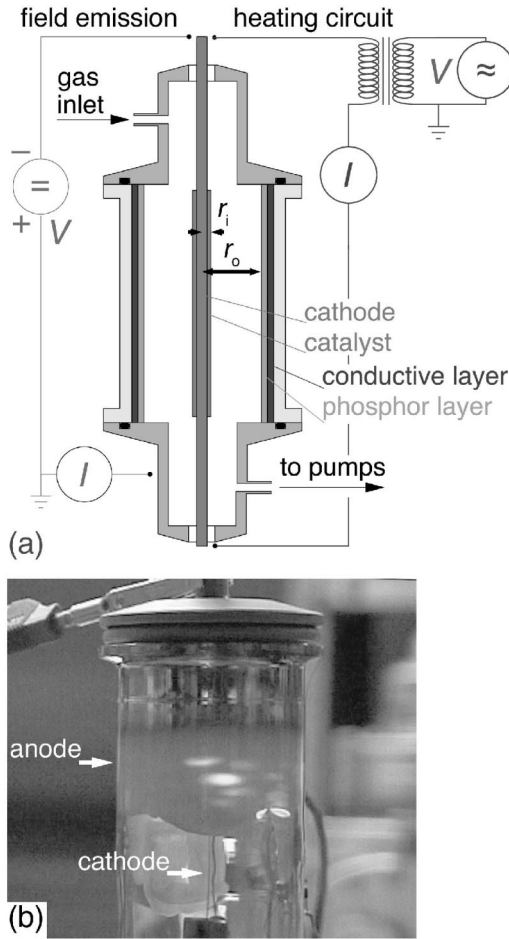


FIG. 1. (a) Schematics and (b) photograph of the experimental setup used to study the CVD growth of nanotubes by field emission. Individual emitting nanotubes are visible as single elliptical patterns on the phosphor screen in (b).

$$I = A \frac{1.5 \times 10^{-6}}{\phi} \left( \frac{V}{d} \right)^2 \gamma^2 \exp\left( \frac{10.4}{\sqrt{\phi}} \right) \exp\left( \frac{-6.44 \times 10^9 \phi^{1.5} d}{\gamma V} \right). \quad (3)$$

$\gamma$  is an important parameter for field emission and can be determined from the measurements with a so-called F-N plot, where  $\ln(I/V^2)$  is given versus  $1/V$ .<sup>15,16</sup> Alternatively,  $\gamma$  can be estimated from the geometry: for nanotubes, one can use the models<sup>20</sup> developed for a cylinder of height  $h$  terminated by a half sphere of radius  $r$  on a flat surface, which state that<sup>21</sup>

$$\gamma \approx 0.7 \times h/r \quad (4)$$

when  $h$  is far smaller than the interelectrode distance.

As we will see in Sec. IV, our field-emission measurements are performed in a cylindrical geometry, as opposed to the usual plan-to-plan or plan-to-sphere configurations. The nanotubes are deposited on a wire of radius  $r_i$  which is placed at the center of a cylindrical anode of radius  $r_o$ , as shown on Fig. 1(a). We have shown that the Fowler-Nordheim model can still be used in this case, provided that the electric field is written as  $E(r) = V/[r \ln(r_o/r_i)]$  instead

of  $E = V/d$  for two planar electrodes.<sup>22</sup> This in turn implies that the interelectrode distance used in Eqs. (3) and (4) has to be taken as  $d = r_i \ln(r_o/r_i)$ .<sup>22,23</sup>

### III. CVD GROWTH OF CARBON NANOSTRUCTURES

The growth of carbon nanotubes by CVD involves the thermal decomposition of a hydrocarbon gas at the surface of a transition-metal catalyst particle and/or at a hot filament or in a plasma. The carbon diffuses then through (or over) the particle and segregates in a  $sp^2$  structure, which ultimately leads to the formation of a nanotube. Several CVD techniques have been demonstrated over the past several years. Thermal CVD is a simple pyrolysis, usually performed in a flow reactor inside a tubular oven. The CVD process can also be assisted by a hot filament (hot filament CVD),<sup>24</sup> and/or by a microwave or rf plasma (plasma-enhanced CVD).<sup>25,26</sup> The latter two embodiments are more complicated but allow to decrease significantly the growth temperature and adjust more flexibly the reaction atmosphere.<sup>27</sup> We have demonstrated recently another variation of CVD which will be presented in more detail in the next section.

The CVD growth of carbon nanotubes is an extremely complex phenomenon in which several parameters play an important role. First, the chemical nature and composition of the carbonaceous gas phase has undoubtedly an influence on the outcome of the growth, and the situation is not simple since nearly every research group uses slightly or completely different approaches (thermal, hot-filament, and plasma-assisted CVD of  $C_2H_2$ ,  $CH_4$ , and/or  $CO$  with often  $H_2$  and/or  $NH_3$  as dilution gases). Second, the temperature of both gas phase and substrate play a role. Third, the chemical nature of both catalyst precursor (sputtered metal thin film, metallic ions in solution, well-defined particles) and catalyst active phases (unknown at present) have an impact on the quality of the grown structures<sup>28</sup> and can be also influenced by the gas phase and/or temperature.<sup>29</sup> Finally, the particle diameter determines to a large extent (but not unequivocally) the tube diameter, and the support and support-catalyst interactions can also influence drastically the outcome of the growth.

The direct observation of CVD growth is an obvious solution to provide clues to the above questions, but it has to our knowledge been attempted only by one group. Baker *et al.* developed “controlled atmosphere electron microscopy” in the 1970s, where partial pressure of hydrocarbons is introduced in the column of a transmission-electron microscope equipped with a heating probe holder.<sup>30</sup> Baker *et al.* found that the diameter is controlled by the size of the catalyst particle, and that the growth rate is linear after a period of activation and remains linear until the growth stops. They also observed growth in excess of  $1\text{-}\mu\text{m}$  length at  $740^\circ\text{C}$  with 3 mbar of  $C_2H_2$  and found an increase of the growth rate when the particle diameter is decreased, which points to a diffusion-controlled growth mechanism (i.e., the diffusion of C through the particle is the rate-limiting step). The growth rate they deduced with particles of 20-nm diameter is  $55\text{ nm/s}$ .<sup>30</sup> The method we demonstrate in the next sections

uses a simpler experimental setup, is more flexible, and allows also to observe the structures during the CVD growth.

#### IV. EXPERIMENTAL SETUP

The experimental technique we use to follow the growth of nanotubes originates from the development of luminescent tubes based on carbon nanotube field emission.<sup>22</sup> In such elements, the cathode is a wire that supports the nanotubes and is placed in the center of symmetry of a glass tube coated with a phosphor layer that serves as anode, as in Fig. 1. In a first phase, the nanotubes were grown on the wire by thermal CVD,<sup>22,31</sup> but the length of the cathodes was limited to  $\sim 10$  cm for usual CVD systems, since the support has to be heated homogeneously. To circumvent this problem, we developed “cold atmosphere CVD,” (CACVD):<sup>32,33</sup> as shown in Fig. 1(a), the growth is carried out in the final device on wires of Kanthal (an Fe-Al-Cr alloy), which allows to control the growth of nanotubes by the deposition of a catalytic solution of iron nitrate [ $\text{Fe}(\text{NO}_3)_3 \times 9\text{H}_2\text{O}$ ] in ethanol.<sup>31</sup> The CVD growth is activated by heating the wire resistively to typically  $700^\circ\text{C}$  and introducing a hydrocarbon partial pressure in the chamber. We have shown that high quality nanotubes can be grown under 1–400 mbar of  $\text{C}_2\text{H}_2$  when the wire was heated to  $700^\circ\text{C}$ , on up to  $950^\circ\text{C}$  (as measured with an optical pyrometer).<sup>32</sup> It is worth noting that nanotubes grow only if a catalyst is present on the support, if the support is heated, and if a partial pressure of a hydrocarbon gas is present around the heated support. The deposition can be stopped by cooling the wire and/or removing the partial pressure of hydrocarbons through the vacuum pumps.

The configuration of CACVD as displayed in Fig. 1 allows to measure the field emission as soon as the hydrocarbon partial pressure has been evacuated by the vacuum pumps after the growth. Furthermore, the growth can be resumed directly if the field-emission performances are not satisfactory. Thereupon came the idea of combining the two distinct phases of the experiment, i.e., of performing field emission *in situ* during the growth.<sup>23</sup>

How can such a setup be used to monitor the growth of nanotubes in real time? Since the length of nanotubes increases as the growth proceeds, the field-enhancement factor,  $\gamma$ , also increases with time. Our idea was to use this fact to monitor the growth, by detecting the field-emitted current from one or an assembly of tubes *during the growth*. To this effect, two main modifications had to be carried out with respect to the usual CACVD growth setup.<sup>32</sup> First, a high voltage has to be applied during the growth, which means that the circuit used to resistively heat the support to the growth temperature has to be decoupled from the electrical ground to avoid ground loops and to maintain a low noise level during the measurements. This was done by using a transformer, with the primary loop connected to an ac voltage source and the secondary loop connected to the support, which keeps the support at a floating potential with respect to the electrical ground. A high positive voltage was applied to the anode to extract electrons and the support itself was grounded through an electrometer (Keithley 617A). The second modification enables to apply the few kV necessary to

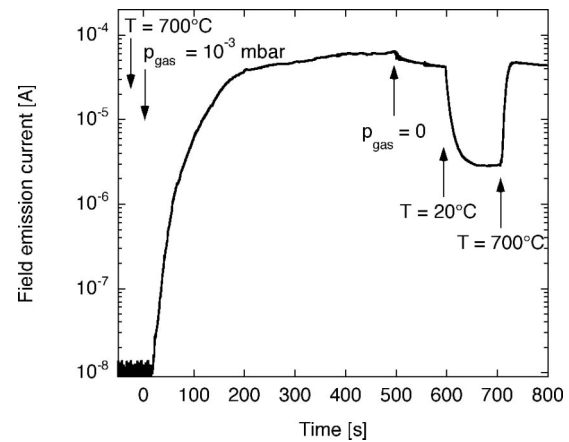


FIG. 2. Emitted current vs time ( $I$ - $t$ ) curve for a CACVD growth carried out at  $700^\circ\text{C}$  under  $10^{-3}$ -mbar  $\text{C}_2\text{H}_2$  introduced at  $t=0$  with 3-kV applied voltage.

reach field emission, and consists in a decrease of the  $\text{C}_2\text{H}_2$  partial pressure in the chamber during growth below  $10^{-2}$  mbar to avoid plasma discharges.

For all measurements, we used a glass tube of 21-mm inner radius with a conductive indium tin oxide (ITO) layer as the anode. The phosphor is either a NP1045 from Nichia for white light or a P22 from Osram for high intensity green light, and is deposited on the ITO layer inside the glass tube by standard techniques. The Kanthal support wires of 0.15-mm radius and 10-cm length are cleaned in acetone and ethanol before oxidation in air at  $1000^\circ\text{C}$  for 12 h.<sup>22</sup> The Fe-based catalyst [ $20$  mM of  $\text{Fe}(\text{NO}_3)_3 \times 9\text{H}_2\text{O}$  in ethanol] is delivered onto the metallic wire by dipping, so that the effective length of the cathode (i.e., the active part of the cathode for growth and field emission) is 5 cm, yielding an emission area of  $0.5\text{ cm}^2$ . After evacuating the setup down to  $10^{-7}$  mbar, the wire is heated at  $950^\circ\text{C}$  during 15 min as measured with an optical pyrometer. The temperature is then lowered to the growth temperature of  $700^\circ\text{C}$ , a high voltage of 3 kV is applied, and a partial pressure of  $\text{C}_2\text{H}_2$  is introduced in the chamber. The growth is stopped by evacuating the hydrocarbon gas and cooling the wire.

#### V. RESULTS AND DISCUSSION

##### A. Monitoring the growth of nanotube arrays

Figure 2(a) shows the outcome of a typical experiment. A potential difference of 3 kV was applied at the beginning of the experiment, and the wire was heated to  $700^\circ\text{C}$  for 30 s before the  $\text{C}_2\text{H}_2$  was introduced. A field-emitted current was detected after 22 s, and increased sharply in the first three minutes of the growth. The  $\text{C}_2\text{H}_2$  was evacuated after 500 s, which induced a 20% decrease of the current while the noise level diminished by a factor of 3. The wire was cooled down at 600 s, which provoked a further decrease of the current. This decrease was reversible, since heating the wire up to the growth temperature brought the current back up to its former value (see also Fig. 5 below). We might conclude from Fig. 2 that the growth begins simultaneously for all nanotubes after a short activation time, then proceeds with a homogeneous

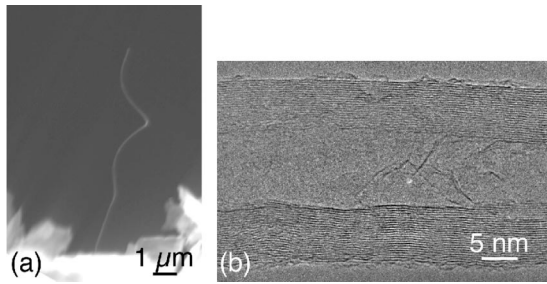


FIG. 3. (a) Scanning and (b) transmission-electron microscopy micrographs of nanotubes grown by CACVD during an experiment comparable to the one shown in Fig. 2.

lengthening that is detected by the increase in field-emission current and is interrupted after some time. Indeed, a subsequent observation of the cathodes using scanning electron microscopy (SEM) and transmission-electron microscopy (TEM), as shown in Fig. 3, reveals that well-graphitized multiwall carbon nanotubes of typically 5–10-nm radius and at least 10- $\mu$ m length are produced.

The configuration of the experiment (see Fig. 1) makes it possible not only to measure the emitted current, but also to visualize its spatial distribution. When a phosphor screen is used as the counterelectrode, the obtained pattern allows to identify individual emitters [such as the spots visible in Fig. 1(b)] as well as infer the presence (or absence) of adsorbates. Note that this technique, field-emission microscopy (FEM), has been extensively used in the past 60 years in surface science.<sup>15,34,35</sup>

Another experiment is presented in Fig. 4, and the  $I-t$  curve is at first glance comparable to the view of Fig. 2. The video frames acquired during the growth and shown in Fig. 4(b) reveal, however, that the phenomena involved are more complex than described above. First, the growth of the emitters is neither simultaneous nor homogeneous. The first nanotube is detected after 20 s (unfortunately on the other side of the anode), which corresponds to the onset of the emission current. The number of emitters remains low (less than 20 over the 0.5-cm<sup>2</sup> cathode) in the first phase as the current increases by four orders of magnitude. The emitter density increases then markedly from 50 s on as the current increases becomes linear, and continues to increase slightly after the maximal current is reached at 180 s.

There are a few puzzling points in the results presented in the preceding figures. First, the emission images have an elliptical shape that is always oriented with the long axis perpendicular to the axis of the cathode, which is rather unexpected. In FEM, the patterns detected on the phosphor screen correspond to a magnified image of the spatial distribution of the emitted current at the tip, since the emitted electrons follow initially the field lines just after tunneling into the vacuum.<sup>36</sup> Since the nanotubes have a circular cross section, one usually observes a circular emission image,<sup>37</sup> a ring for an opened tube,<sup>37</sup> well-defined two- or four-lobed patterns that correspond to adsorbates,<sup>38</sup> or a finer structure that reflects the structural arrangement and/or electronic properties of the nanotube cap.<sup>39,40</sup> We surmise that the elliptical shape observed in Fig. 4(b) is an effect of the cylin-

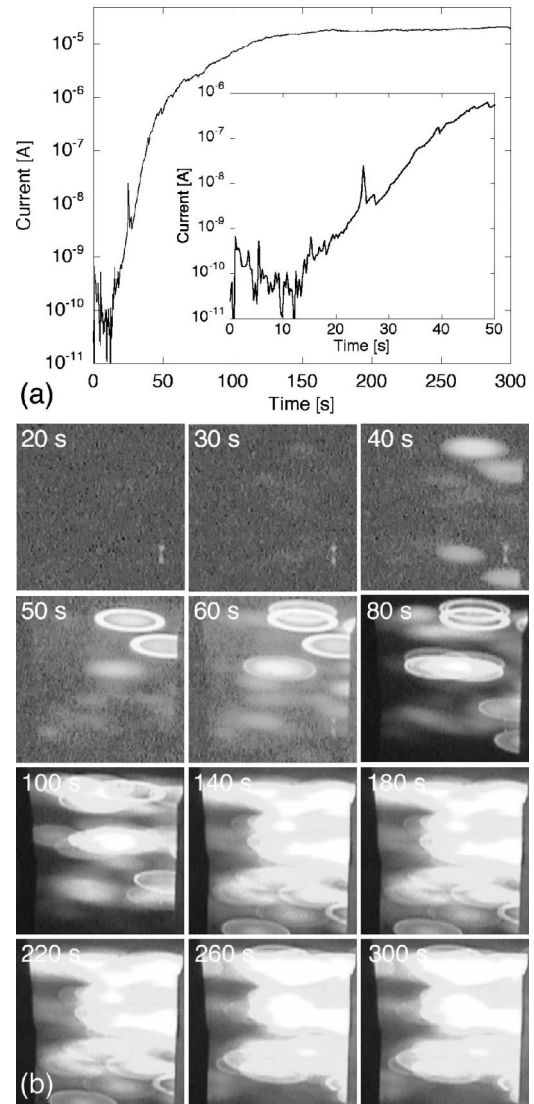


FIG. 4. CACVD growth carried out at 700 °C and  $10^{-4}$  mbar  $C_2H_2$  introduced at  $t=0$  under 3-kV applied voltage. (a) Emitted current vs time ( $I-t$ ), with (inset) the first 50 s; (b) video frames of one-eighth of the anode acquired during the growth (the contrast of the first frames has been enhanced). The two small points on the lower right-hand side in the first images are a reflection on the glass tube and are not related to the growth.

drical geometry. The magnification of the emission image depends on the shape of the equipotentials around the tip: the equipotentials follow closely the shape of the tube apex for an infinitely long nanotube, but show a larger radius of curvature as the length of the nanotube decreases because of shielding due to the support.<sup>21,41</sup> In our case, the shape of the equipotentials is not symmetric with respect to the axis of the nanotube. Their radius of curvature at the tip is smaller in the plane perpendicular to the wire than in the parallel direction, since the cross section of the support surface is a circle as opposed to a slab. This difference in curvature produces the elliptical shape, as the magnification is highest for the electrons emitted in the plane perpendicular to the wire and lowest in the orthogonal direction.

Second, most emitters appear over less than 10 s, as can be seen by comparing subsequent images in Fig. 4(b), and not all of them emit over the whole duration of the experiment. For example, the two tubes that appear between 100 and 140 s at the bottom of the frames in Fig. 4(b) disappear abruptly after 220 s. We examine this behavior in more detail in the next section.

### B. Monitoring the growth of individual nanotubes

Two kinds of patterns are found in the images of Fig. 4(b), namely, homogeneous spots (e.g., the topmost nanotube at 40 s) and central patterns (mostly homogeneous) surrounded by a well-defined ring (e.g., the same tube at 50 s). Growing nanotubes present a single, homogeneous spot. Since opened tubes produce rings or arcs without any central spot,<sup>37</sup> this indicates clearly that the growth proceeds with a closed cap and the cap is not significantly modified during the growth. The single spot could be due either to the clean cap<sup>39</sup> or to an adsorbate,<sup>40</sup> but the temperature used for the growth makes the latter possibility unlikely, since most adsorbates desorb around 600 °C.<sup>38</sup> It is also probable that the cap is the first part of the nanotube to be formed, as opposed to a mechanism where the cylindrical part of the tube grows with an opened end that may be closed as the growth stops. This is supported by transmission-electron microscopy observations, since the catalyst particles remain attached to the substrate in 90% of the tubes. The great majority of the nanotubes we observe, with the support, catalyst, and deposition parameters used, have therefore been obtained by “root growth.”

After the end of the growth, we systematically observe a ring in addition to the central spot. As shown in Fig. 5, this ring appears at high temperature on all nanotubes and disappears reversibly when the nanotubes are cooled, along with a change in the current by a factor 3. Such rings have been observed on metallic emitters, as well as on single-walled nanotubes by Dean *et al.*<sup>39</sup> It is probable that this ring and the increase in current are due to thermally assisted emission. The temperature of 700 °C is usually not sufficient to induce thermoelectronic emission from materials with a work function of 5 eV. However, the field-emitted current heats the emitter resistively<sup>42</sup> and probably contributes to an increase of the temperature that is sufficient to reach the threshold of a mixed field-emission–thermoelectronic emission regime.

As we have seen in Fig. 4, the growth of most emitters is fast (typically 10–15 s). We have observed single nanotube growths stretching over more than 30 s, but these were exceptions. We also found that the duration of the growth was different for every nanotube, with differences of up to a factor 5. It is at present difficult to conclude if this is due to differences in growth rate or to different final lengths.

An example of a very short growth is shown in Fig. 6, and is taken from the experiment depicted in Fig. 4. The emission image is homogeneous, becomes brighter as the emitted current increases, then disappears abruptly. It appears by comparing the  $I-t$  curve in the inset of Fig. 4(a) with the video frames of Fig. 6, in which the apparition and increase in intensity of the emission image correspond to the sharp increase in current 24 s after introduction of the  $C_2H_2$ . Fur-

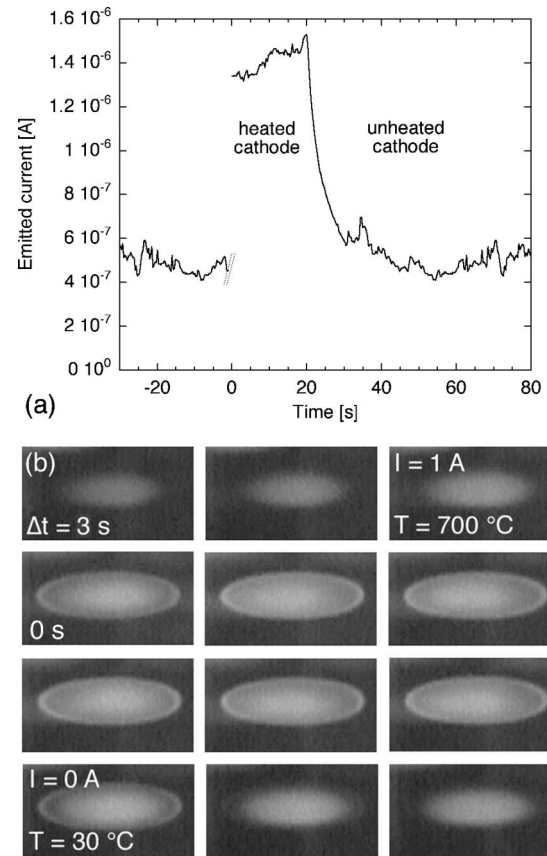


FIG. 5. (a) Emitted current versus time ( $I-t$ ) for an applied voltage of 3 kV during a heating-cooling cycle, with (b) corresponding video frames acquired at 3-s intervals.

thermore, the disappearance of the emission image and the drop in emission current are simultaneous, which indicates that the event corresponds to the destruction of the emitter. We suspect that this behavior is due to the fact that the emitted current increases steadily as the growth proceeds and

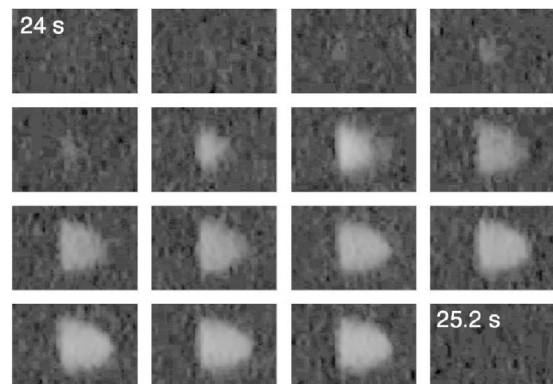


FIG. 6. Video frames of a single nanotube acquired during the growth at 700 °C and  $10^{-4}$  mbar  $C_2H_2$  introduced at  $t=0$  under 3 kV applied voltage corresponding to the sudden increase and decrease in current shown in the inset of Figure 4(a). The interval between the frames is 0.08 s. The phosphor layer is applied in vertical bands, so that only the right half of the emission images has been detected.

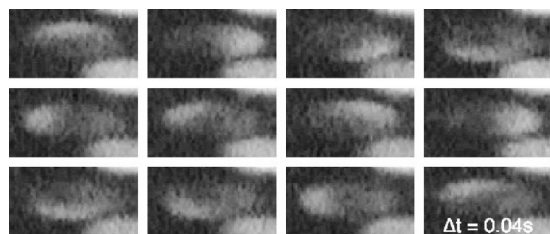


FIG. 7. Video frames showing the modification of the field-emission pattern of an individual nanotube grown at 700 °C and  $10^{-4}$ -mbar  $C_2H_2$  under 3-kV applied voltage. The interval between the frames is 0.04 s.

may reach a current density that destroys the emitter.<sup>14</sup> This limit amounted to 20 nA for the nanotube shown in Fig. 6, which is readily comparable to the values obtained in measurements carried out in the scanning electron microscope on individual CVD-grown nanotubes.<sup>43</sup> This behavior was frequently observed, since the increase in current during the first phase of the growth was not monotonous but showed a series of increases and abrupt decreases [one other example is given in Fig. 9(b) below]. We estimate that about one out of eight nanotubes survive beyond 10 s of growth.

In such cases, the growth was terminated before a critical current density was reached. The mechanisms leading to the interruption of the growth are not yet clear, although they probably involve a poisoning of the catalyst,<sup>30</sup> i.e., a change in the chemical composition or crystallographic structure that diminishes its catalytic activity. The active catalytic phase is yet unknown for CVD-grown carbon nanotubes. Twenty years of research on carbon fiber CVD growth have yielded two different interpretations, namely, catalysis by metals or by carbides. Researchers studying the decomposition of  $C_2H_2$  and  $C_2H_4$ , i.e., in conditions similar to the ones used here, found that the active catalyst is the pure metal [mostly  $\gamma$ -Fe (fcc), but also  $\alpha$ -Fe (bcc) (Ref. 44)] or the metal oxide, and that the carbides do not catalyze the growth. It seems that the catalyst is poisoned by carbonization.<sup>45</sup> This poisoning is thought to occur when the diffusion through the particle is not sufficient to transport all the carbon atoms produced by the hydrocarbon decomposition, which leads to a decrease of the active surface area and ultimately the end of the growth.

Another class of observed effects were movements and modifications of the pattern, which appeared on some tubes after termination of the growth. An example is given in Fig. 7: the emission image is no longer homogeneous but shows a strong spot that revolves quickly (clockwise in the case of Fig. 7) around the circumference of the pattern. These movements were always fast, and random in speed and direction (halts and inversions were frequent). These phenomena could be due to structural rearrangements or modifications of the nanotube cap,<sup>46</sup> or to adsorbate movement. The former possibility is more likely, since the emitters were heated at high temperature and patterns typical of adsorbates<sup>15,38,40</sup> were not observed on cathodes during or immediately after growth. Conversely, adsorbates were detected on “old” cathodes, e.g., after a prolonged time in vacuum at room temperature or after exposition to the ambient atmosphere.

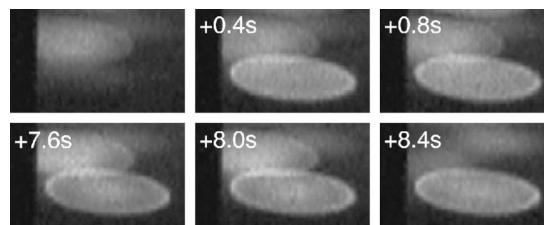


FIG. 8. Video frames acquired during the growth of nanotubes at 700 °C and  $10^{-4}$ -mbar  $C_2H_2$  under 3-kV applied voltage. The time elapsed since the first frame is indicated.

Finally, we also observed behaviors that did not compare with those described above. An example is shown in Fig. 8, where patterns appear and disappear in less than 0.04 s. Usually, a pattern appears gradually when the nanotube is growing, and disappears abruptly as the intensity increases in the case of a destruction during the growth. Both occurrences are abrupt in Fig. 8, and we suggest that these events arise because of modifications of the surroundings of the emitters, and not modifications of the emitters themselves. Field emission is extremely sensitive to the applied field, and therefore to both applied voltage and field-enhancement factors. The latter parameter is critically influenced by the diameter and length of the nanotubes, but also by the spacing between the nanotubes,<sup>47</sup> and more generally by the presence or absence of neighboring tubes. The disappearance of an emitting nanotube (last frame of Fig. 8) can simply be due to another nanotube that grows in its immediate vicinity and shields the applied field, thereby decreasing the field enhancement and therefore the emitted current. As the emitted current increases nonlinearly with the field, small changes in  $\gamma$  can provoke huge variation in the current and hence the abrupt disappearance of an emitter. Another possibility is the adsorption or desorption of molecules which modify the electronic structure of the emitting states. Sudden apparitions (such as in the second frame of Fig. 8) probably occur due to similar reasons.

### C. Estimating the growth rate

The growth rate is a crucial parameter to control the length of the nanotubes, and is a parameter on which the available information is scarce. For plasma-enhanced CVD of  $C_2H_2:NH_3$ , values of 8–16 nm/s (2-mbar gas pressure, 750 °C)<sup>48</sup> and 100 nm/s (20 mbar, 825 °C) (Ref. 49) have been determined, but in both cases for large diameter nanotubes (40 nm) and in a reaction atmosphere that contained atomic hydrogen, which means that the structures resulted from a balance between CVD growth and reactive etching by the hydrogen. In thermal CVD where no atomic hydrogen is present, we inferred a growth rate of at least 150 nm/s from 10- $\mu$ m-long nanotubes that grew in 1-min deposition.<sup>50</sup> In all these studies, the nanotube films were examined *after* the growth, and the growth rates were extracted by dividing the increase in length of the nanotubes by the difference in growth time between two different samples. The estimated growth rate is therefore only a lower limit, since it was impossible to conclude whether the growth of a nanotube oc-

curs over the whole time of exposition to the hydrocarbon gas, or only over a far shorter time scale.

The only studies in which the growth rate has been determined by direct observation have been performed by Baker *et al.* The length of filaments grown by CVD of  $C_2H_2$  over Fe catalysts increased linearly after a period of initiation of a few seconds until the termination of the growth through poisoning of the catalyst after typically 60 s.<sup>30</sup> The growth rate increased with decreasing catalyst particle (and filament) diameter, with a maximal growth rate of 65 nm/s for 20-nm-diameter filaments.<sup>30</sup> Finally, growth rates of nearly 3  $\mu\text{m/s}$  were observed for PtFe catalysts.<sup>51</sup>

Our results suggest clearly that the growth rate of the emitters is quite high: we estimate the growth time for most nanotubes in Fig. 4 to be 10–20 s, with even much shorter duration some exceptional cases as in Fig. 6. Since the final length of the nanotubes is of at least 10  $\mu\text{m}$  as estimated by SEM and TEM, the actual growth rate is probably on the order of 0.5–1  $\mu\text{m/s}$ .

We estimate in the following the growth rate directly from the  $I$ - $t$  curve. Equation (4) shows that the field enhancement depends linearly on the length of the emitter. If we assume, as for carbon filaments,<sup>30</sup> that the growth rate is constant and hence the length increases linearly, then the field-enhancement factor will also increase linearly with time. We write therefore that the field enhancement factor increases as  $\gamma(t) = \Gamma(t - \Delta t)$ , where  $\Gamma$  is the rate of increase of  $\gamma$  and  $\Delta t$  is the activation time. We then introduce this dependence in the Fowler-Nordheim law in Eq. (3), and obtain the following expression for  $I$ :

$$I = A \frac{1.5 \times 10^{-6}}{\phi} \left( \frac{V}{d} \right)^2 [\Gamma(t - \Delta t)]^2 \exp\left( \frac{10.4}{\sqrt{\phi}} \right) \times \exp\left[ \frac{-6.44 \times 10^9 \phi^{1.5} d}{\Gamma(t - \Delta t)V} \right]. \quad (5)$$

We take in the following  $\phi = 5$  eV for the work function, which is a good approximation for carbon nanotubes.<sup>17,52</sup>  $V$  is constant during the experiment (usually,  $V = 3$  kV) and  $d = r_i \ln(r_o/r_i) = 0.75$  mm in our case ( $r_o = 21$  mm,  $r_i = 0.15$  mm).<sup>22</sup> Equation (5) therefore gives us a  $I$  versus  $t$  dependence with  $A$ ,  $\Gamma$ , and  $\Delta t$  as variables. We estimate these parameters by fitting the experimental  $I$ - $t$  curves with Eq. (5) using the package NONLINEARFIT of the Software Mathematica version 4.1 from Wolfram Research Incorporated.<sup>56</sup> The consistency of the results was checked by performing the fitting over different portions of the same  $I$ - $t$  curve, and deviations of 10% were found for  $\Gamma$ .  $\Delta t$  was forced to equal 0 when the fitting yielded a negative value.

We display in Fig. 9 two examples of fitting Eq. (5) to experimental  $I$ - $t$  curves for a growth over the whole cathode [Fig. 9(a)] and an event related to the growth and subsequent destruction of an individual tube [Fig. 9(b)]. For the whole growth of Fig. 9(a), we obtained  $\Gamma = 200 \text{ s}^{-1}$  and  $\Delta t = 11$  s, and  $\Gamma = 720 \text{ s}^{-1}$  and  $\Delta t = 13$  s for Fig. 9(b). Our simple model fits well the experimental data from the beginning of the increase in current over more than four orders of

magnitude. The experimental behavior deviates from the model when individual tubes are destroyed by high current densities, or, for measurements taken over the whole cathode, when the growth of the first emitters has been interrupted and subsequently growing nanotubes contribute only to a linear increase of the current. The field-enhancement factors of the fully grown nanotubes deduced from the fits,  $\gamma = 8125$  for Fig. 9(a) and  $\gamma = 5500$  for Fig. 9(b), correspond well to the field enhancement factors deduced from F-N plots acquired after the growth (not shown here<sup>22</sup>).

Interestingly, the results indicate in both cases an activation time of  $\sim 10$  s. The very beginning of the growth cannot be observed in our measurements since the emitted current is below the noise level in the first 3–8 s of the growth. To observe the very beginning of the growth, one should apply a sufficiently high voltage to observe field emission from the support, which means, however, that the growing emitters are likely to be destroyed after shorter durations.

Similar results were obtained for the experiments with activation times below 15 s and  $\Gamma$  between 135 and  $1130 \text{ s}^{-1}$  for the whole  $I$ - $t$  curves: the other examples shown here yielded  $\Gamma = 170 \text{ s}^{-1}$  and  $\Delta t \approx 0$  s for Fig. 2, and  $\Gamma$

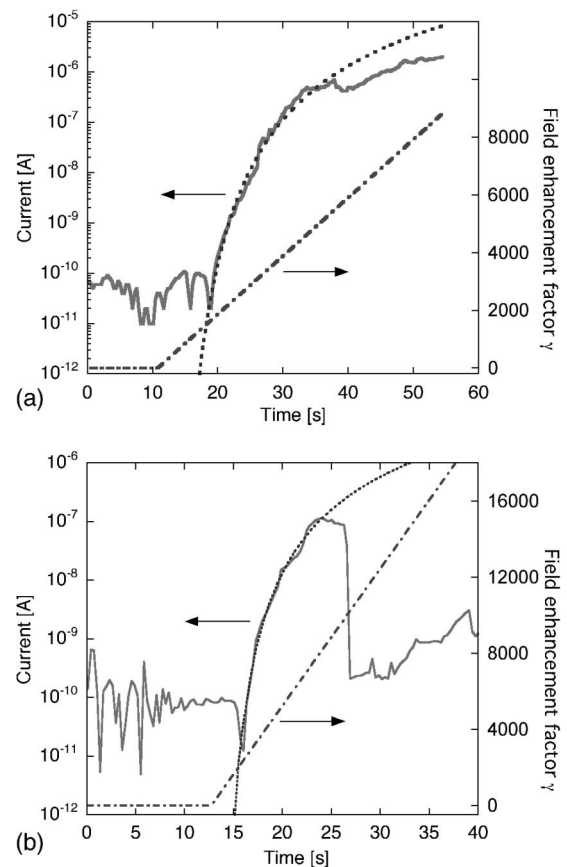


FIG. 9. Emitted current vs time ( $I$ - $t$ ) curves (plain lines) and corresponding fits to Eq. (5) (dotted lines) along with the field-enhancement factor (dash-dotted lines) for growth carried out at  $700^\circ\text{C}$  with (a)  $10^{-3}$ -mbar and (b)  $10^{-4}$ -mbar  $C_2H_2$  introduced at  $t = 0$  under 3-kV applied voltage. The fitting has been done in (a) for the whole growth and in (b) for a single tube event similar to the one shown in Fig. 6.

$=270 \text{ s}^{-1}$  and  $\Delta t \approx 0 \text{ s}$  for Fig. 4. For events that can be traced back to single tubes such as the one shown in Fig. 6,  $\Gamma$  varied between 130 and  $720 \text{ s}^{-1}$ , with field-enhancement factors that amounted to 2000–8000 just before the destruction of the emitter.

Fitting Eq. (5) to the measurements yields the rate of increase of  $\gamma$ , and not directly the growth rate. To relate  $\Gamma$  to the growth rate, we need an analytical expression for  $\gamma$ . For planar geometry, Eq. (4) states that  $\gamma \approx 0.7 \times h/r$ .<sup>21,14</sup> However, this expression will overestimate the growth rate in cylindrical geometry, since  $\gamma$  is higher than in the planar case with the same  $h$  and  $r$ . We therefore obtain an upper limit for the growth rate, with further uncertainty since the radius of the nanotubes has to be estimated and probably varies from one emitter to the next. If we take  $r = 5 \text{ nm}$  as suggested by Fig. 3, we obtain growth rates of 0.95 to  $8 \mu\text{m/s}$  for the whole growth, and 0.9 to  $5 \mu\text{m/s}$  for the individual tubes. This estimate yields nanotube lengths in excess of  $10 \mu\text{m}$  for the fully grown nanotubes, which corresponds to the SEM and TEM observations.

These estimates are considerably higher than the rare reliable values published in the literature (see above and Refs. 48, 49, and 30). One significant difference is that the growth is carried out with an applied electric field which causes variations in the growth process. On one hand, some setups for hot-filament CVD (Ref. 54) use an electric field to promote the growth, and the electric field is naturally present in plasma-assisted CVD.<sup>55</sup> A field has also been used in thermal CVD (Ref. 53) to control the direction of growth and align nanotubes, e.g., between two electrodes. It is also well known that nanotubes react strongly to an applied field, resulting in an alignment perpendicular to the substrate for low applied voltages.<sup>14</sup> On the other hand, Bower *et al.* found a 40-times higher growth rate on the same sample with plasma-enhanced (applied field) as opposed to thermal CVD (no applied field), which could be due to the difference in the composition of the reaction atmosphere. In our case, we found that the voltages needed to reach a given current density were far higher without applied field during CACVD growth as compared to the conditions described in this study.

The partial pressure of  $\text{C}_2\text{H}_2$  used in this study was varied between  $10^{-4}$  and  $10^{-2}$  mbar, which are, respectively, the lower limit for growing nanotubes and the higher limit for applying the high voltage and not initiating a discharge. We found variations of the growth rate and activation time, but the spread in the values is quite large, and it is probable that other parameters (especially regarding the preparation of the catalyst) play an important role in the growth. It is difficult to assess precisely the activation time of the catalyst, since we cannot observe the very beginning of the growth and are able to detect a current only for nanotubes that have at least  $\gamma \geq 2000$ . It seems nevertheless that the time between the introduction of the  $\text{C}_2\text{H}_2$  and the first detected increase in current decreases with increasing pressure from 10–126 s down to 10–12 s. The time between the beginning of the growth and the saturation also decreases markedly with increasing pressure, even if there are large variations from one experiment to the next.

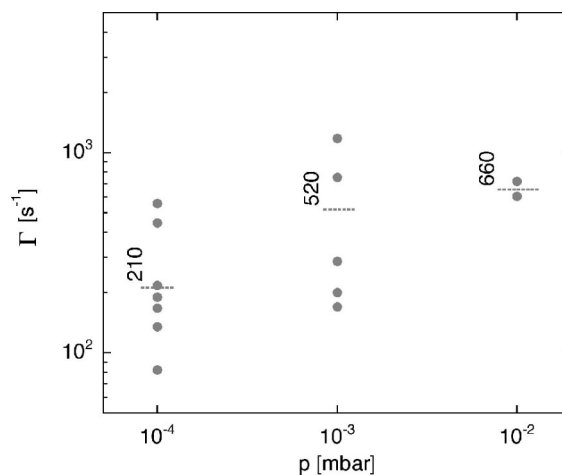


FIG. 10. Rate of increase of the field-enhancement factor,  $\Gamma$ , as a function of  $\text{C}_2\text{H}_2$  pressure, as determined by fitting Eq. (5) to the  $I$ - $t$  curves.

Figure 10 shows the influence of the pressure on  $\Gamma$ . The average growth rate increases with the pressure from  $\Gamma = 210$  to 520 and 660  $\text{s}^{-1}$  for  $10^{-4}$ ,  $10^{-3}$ , and  $10^{-2}$  mbar, respectively. This corresponds to maximal growth rates ( $r = 5 \text{ nm}$ ) of 1.5, 3.7, and  $4.7 \mu\text{m/s}$ . We consider the implications of these high growth rates by taking as an example a rate of  $1 \mu\text{m/s}$ . A multiwall nanotube has essentially the same density as turbostratic graphite, which means that a nanotube of length  $h$ , with inner and outer radii  $r_{\text{in}}$  and  $r_{\text{out}}$ , will weigh  $m = \rho \pi (r_{\text{out}}^2 - r_{\text{in}}^2) h$  where  $\rho = 2.25 \text{ kg/dm}^3$  is the density of graphite. Conversely, the nanotube will be composed of  $m \times N_A / m_M = \rho \pi (r_{\text{out}}^2 - r_{\text{in}}^2) h N_A / m_M$  carbon atoms, where  $m_M = 0.012 \text{ kg/mol}$  is the molar mass of carbon and  $N_A = 6.023 \times 10^{23} \text{ mol}^{-1}$  is Avogadro's number. A nanotube of  $r_{\text{in}} = 2.5 \text{ nm}$ ,  $r_{\text{out}} = 5 \text{ nm}$  [cf. Fig. 3(b)] therefore weighs  $0.13 \text{ fg}$  per  $\mu\text{m}$  and is composed of 6.7 million C atoms per  $\mu\text{m}$ . This means that at least 3.35 million  $\text{C}_2\text{H}_2$  molecules ( $5.5 \times 10^{-18} \text{ mol}$ ) are needed per second to sustain a growth rate of  $1 \mu\text{m/s}$ .

In CVD, the hydrocarbon molecules are adsorbed on the catalyst particle (and on the support and/or growing nanotube) and subsequently decomposed by the catalyst. We estimate the number of molecules impinging from the gas phase on a catalyst particle of 10-nm diameter by making the assumption that the whole surface of the particle is available for adsorption. The number of molecules impinging on a surface can be written as  $p / \sqrt{2 \pi m k T} \text{ m}^{-2} \text{ s}^{-1}$ , where  $p$  is the pressure,  $m$  the mass of the molecules ( $4.32 \times 10^{-26} \text{ kg}$  for  $\text{C}_2\text{H}_2$ ),  $k = 1.38 \times 10^{-23} \text{ J/K}$  Boltzmann's constant, and  $T$  the temperature. This amounts to  $1.18 \times 10^{20} \text{ m}^{-2} \text{ s}^{-1}$  at  $10^{-4}$ -mbar  $\text{C}_2\text{H}_2$  at 1000 K, or to  $\sim 150\,000 \text{ s}^{-1}$  over the whole catalyst particle—which is 20-times too low with respect to the needed value as determined above.

We can draw two consequences from this estimation. First, most of the hydrocarbon molecules used for the growth will not be absorbed directly on the catalyst particle at  $10^{-4}$  mbar, but on the support surface, and will diffuse to the particle before decomposition. The supply of the hydrocarbon molecules is therefore likely to be the rate-limiting

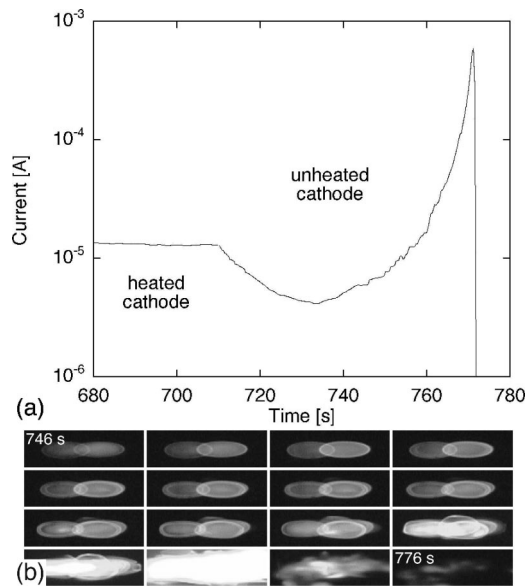


FIG. 11. (a) Emitted current vs time ( $I$ - $t$ ) curve and (b) corresponding video frames taken at 2 s interval of nanotubes grown at  $700^\circ\text{C}$  and  $10^{-4}$ -mbar  $\text{C}_2\text{H}_2$  under 3-kV applied voltage. The  $\text{C}_2\text{H}_2$  has been evacuated, and the heating current was cut at 710 s.

mechanism at such low pressures, which explains the increase in growth rate we observe between  $10^{-4}$  and  $10^{-2}$  mbar. This implies also that decomposition conditions (gas composition, catalyst, support) leading to tip growth (i.e., with the catalyst particle at the tip of the tube) will not allow to sustain the formation of long nanotubes at such pressures, since the surface available for hydrocarbon absorption is too small once the catalyst particle has lifted off from the support surface. Second, the number of hydrocarbon molecules impinging directly on the catalyst particle will be high enough to sustain the growth only at pressures higher than the ones considered here. Baker *et al.* deduced from their measurements at 3 mbar that the growth rate is limited by the diffusion of the carbon through the catalyst particle.<sup>30</sup> we estimate this transition between pressure-limited and diffusion-limited growth to be  $10^{-3}$ – $10^{-2}$  mbar.

#### D. Destruction of emitting tubes

We have noted above that carbon nanotubes are damaged or destroyed during field emission when the current density exceeds a given limit. We describe in this section an event that was observed at the end of a few runs, and that led to the spectacular degradation of nanotubes.

Figure 11 shows the  $I$ - $t$  curve and corresponding video frames of nanotubes emitting after completion of the growth and evacuation of the hydrocarbon partial pressure. The cathode remains heated at  $700^\circ\text{C}$ , and the field-emitted current is stable at  $12\ \mu\text{A}$ . The cathode is then cooled, and a decrease of the current is observed, similar to the ones shown in Figs. 2 and 5. After 20 s, however, the current starts increasing again, and the emission images show a behavior consistent with heating of the emitters (increase of the intensity and apparition of the ring, see Fig. 5), although the cathode remains at room temperature. The current continues to

increase sharply beyond the level reached at high temperature, and the emission images begin to show distorted shapes of increasing dimensions. The increase in current is interrupted abruptly around  $10^{-3}$  A, which corresponds to a big “flash” on the phosphor screen. The images strongly suggest a collective behavior, conversely to the destruction of nanotubes described above, which is always an isolated event unrelated to the emission properties of other nanotubes. The extremely distorted shapes of the emission patterns suggest that the two emitters involved in the event ruptured and that some graphene sheets were progressively detached from the core of the tube. Although the degradation of the emitters is due to the sharp increase in current, we have at present no satisfying explanation for this behavior.

## VI. CONCLUSION

We have monitored the CVD growth of multiwall carbon nanotubes in real time by measuring the field-emission current and characterizing the field-emission patterns of the growing emitters. The increase in length of the nanotubes, and therefore the increase in the field-enhancement factor, are directly reflected in the increase of the emitted current. This allows to observe the nanotubes growing over the whole cathode, to identify events due to the growth and destruction of individual nanotubes, and to estimate the growth rate. Under our deposition conditions, the nanotubes grow with a closed cap with growth rates over  $1\ \mu\text{m/s}$ , the growth rate increases with the  $\text{C}_2\text{H}_2$  pressure, the supply rate of the hydrocarbon to the catalyst particle is the rate-limiting step, and root growth is far more likely.

We are aware that our results may not be directly compared to those obtained under usual CVD conditions. First, the growth is carried out with an applied electric field which may cause variations in the growth process. Second, the partial pressure of hydrocarbons is as low as  $10^{-4}$  mbar, which is at least four orders-of-magnitude lower than usual for CVD, and we have seen that as a consequence the rate-limiting step is not the diffusion of the carbon through the catalyst particle, but rather the supply rate of the hydrocarbon molecules to the particle. Third, the pressure, while very low for CVD, is very high for field emission, which means that molecules from the gas phase may be ionized and bombard the tip.

Nevertheless, our technique allows to obtain precious (and unique) information about the growth. For example, we have noted that the growth of the nanotubes is neither simultaneous nor homogeneous, and that the emitter density remains low in the first minute of exposition to the hydrocarbon gas and increases subsequently afterwards. Subsequent studies will address the influence of temperature, gas mixture, and catalyst on the CVD growth of nanotubes, and we expect significant advances in the understanding of the phenomena related to the growth.

Our technique may also have important technological implications. For field-emission applications, the growth conditions could be tuned and/or modified *during* the growth to match the field-emission properties (emitter and current densities, for example) to the final specifications of the device.

The possibilities are even more enticing for the deposition of a single nanotube, for example, in between the two electrodes of a field effect transistor or on scanning probe microscope tip: the growth can be directed by the applied field and monitored by field emission, and can be stopped as the tube reaches the desired length. Besides the obvious option of monitoring, characterizing, and understanding the growth of nanotubes, our method offers therefore fascinating possibilities for the controlled realization of devices.

## ACKNOWLEDGMENTS

We heartily thank the Center Interdépartemental de Microscopie Electronique of EPFL for access to electron microscopes. Financial support was provided by the Swiss National Science Foundation, the TopNANO21 program, NanoLight International Limited, the European Community, and the Federal Office for Education and Science of Switzerland in the framework of the project CANADIS.

- 
- \*Present address: Rolex S.A., 3-7 rue François-Dussaud, 1211 Genève 24, Switzerland. Email address: jean-marc.bonard@a3.epfl.ch; URL: <http://ipnwww.epfl.ch/nanotubes.html>
- <sup>†</sup>Present address: École d'Ingénieurs du Canton de Vaud, Rte de Cheseaux 1, 1401 Yverdon, Switzerland.
- <sup>‡</sup>Present address: Center Suisse d'Electronique et de Microtechnique SA (CSEM), CH-6055 Alpach, Switzerland.
- <sup>1</sup>M. Dresselhaus, G. Dresselhaus, and P. Avouris, *Carbon Nanotubes* (Springer, Berlin, 2000).
- <sup>2</sup>P. J. F. Harris, *Carbon Nanotubes and Related Structures—New Materials for the Twenty-First Century* (Cambridge University Press, Cambridge, England, 1999).
- <sup>3</sup>R. Andrews, D. Jacques, A. M. Rao, T. Rantell, F. Derbyshire, Y. Chen, J. Chen, and R. C. Haddon, *Appl. Phys. Lett.* **75**(9), 1329 (1999).
- <sup>4</sup>C. Laurent, A. Peigney, O. Dumortier, and A. Rousset, *J. Eur. Ceram. Soc.* **18**(14), 2005 (1998).
- <sup>5</sup>P. G. Collins, M. S. Arnold, and P. Avouris, *Science* **292**, 706 (2001).
- <sup>6</sup>A. Bachtold, P. Hadley, T. Nakanishi, and C. Dekker, *Science* **294**, 1317 (2001).
- <sup>7</sup>H. Dai, J. H. Hafner, A. G. Rinzler, D. T. Colbert, and R. E. Smalley, *Nature (London)* **384**(6605), 147 (1996).
- <sup>8</sup>E. B. Cooper, S. R. Manalis, H. Fang, H. Dai, K. Matsumoto, S. C. Minne, T. Hunt, and C. F. Quate, *Appl. Phys. Lett.* **75**(22), 3566 (1999).
- <sup>9</sup>J. Kong, N. R. Franklin, C. Zhou, M. G. Chapline, S. Peng, K. Cho, and H. Dai, *Science* **287**, 622 (2000).
- <sup>10</sup>S. S. Wong, E. Joselevich, A. T. Woolley, C. C. Li, and C. M. Lieber, *Nature (London)* **394**(6688), 52 (1998).
- <sup>11</sup>S. S. Wong, A. T. Woolley, E. Joselevich, and C. M. Lieber, *Chem. Phys. Lett.* **306**, 219 (1999).
- <sup>12</sup>J.-M. Bonard, H. Kind, T. Stöckli, and L.-O. Nilsson, *Solid State Electron.* **45**, 893 (2001).
- <sup>13</sup>A. M. Cassell, N. R. Franklin, T. W. Tombler, E. M. Chan, J. Han, and H. Dai, *J. Am. Chem. Soc.* **121**, 7975 (1999).
- <sup>14</sup>J.-M. Bonard, K. A. Dean, and B. F. Coll, *Phys. Rev. Lett.* **89**, 197602 (2002).
- <sup>15</sup>W. P. Dyke and W. W. Dolan, *Adv. Electron. Electron Phys.* **8**, 89 (1956).
- <sup>16</sup>J. W. Gadzuk and E. W. Plummer, *Rev. Mod. Phys.* **45**, 487 (1973).
- <sup>17</sup>O. Groning, O. M. Kuttel, C. Emmenegger, P. Groning, and L. Schlapbach, *J. Vac. Sci. Technol. B* **18**(2), 665 (2000).
- <sup>18</sup>I. Brodie and C. Spindt, *Adv. Electron. Electron Phys.* **83**, 1 (1992).
- <sup>19</sup>O. Groning (private communication).
- <sup>20</sup>N. Xu, in *High Voltage Vacuum Isolation*, edited by R. V. Latham (Academic, London, 1995).
- <sup>21</sup>C. J. Edgcombe and U. Valdré, *J. Microsc.* **203**, 188 (2001).
- <sup>22</sup>J.-M. Bonard, T. Stöckli, O. Noury, and A. Chatelain, *Appl. Phys. Lett.* **78**(17), 2775 (2001).
- <sup>23</sup>J.-M. Bonard, M. Croci, F. Conus, T. Stöckli, and A. Chatelain, *Appl. Phys. Lett.* **81**, 2836 (2002).
- <sup>24</sup>A. M. Bonnot, M. N. Semeria, J. F. Boronat, T. Fournier, and L. Pontonnier, *Diamond Relat. Mater.* **9**, 3 (2000).
- <sup>25</sup>Z. F. Ren, Z. P. Huang, J. W. Xu, J. H. Wang, P. Bush, M. P. Siegal, and P. N. Provencio, *Science* **282**(5391), 1105 (1998).
- <sup>26</sup>Z. P. Huang, J. W. Xu, Z. F. Ren, J. H. Wang, M. P. Siegal, and P. N. Provencio, *Appl. Phys. Lett.* **73**(26), 3845 (1998).
- <sup>27</sup>Y. Chen, D. T. Shaw, and L. Guo, *Appl. Phys. Lett.* **76**(17), 2469 (2000).
- <sup>28</sup>C. Klinke, J.-M. Bonard, and K. Kern, *Surf. Sci.* **492**, 195 (2001).
- <sup>29</sup>J.-M. Bonard, K. A. Dean, and B. F. Coll (unpublished).
- <sup>30</sup>R. T. K. Baker, P. S. Harris, R. B. Thomas, and R. J. Waite, *J. Catal.* **30**, 86 (1973).
- <sup>31</sup>O. Noury, M. Croci, T. Stöckli, A. Chatelain, and J.-M. Bonard, *Chem. Phys. Lett.* **346**, 349 (2001).
- <sup>32</sup>M. Croci, J.-M. Bonard, O. Noury, T. Stöckli, and A. Chatelain, *Chem. Vap. Deposition* **8**, 89 (2002).
- <sup>33</sup>M. Croci and J.-M. Bonard, NanoLight International Limited, Patent No. W002068323 (pending).
- <sup>34</sup>R. H. Good and E. W. Müller, *Handbuch der Physik* (Springer, Berlin, 1956), Vol. 21, p. 176.
- <sup>35</sup>R. Gomer, *Surf. Sci.* **299/300**, 129 (1994).
- <sup>36</sup>R. Gomer, *Field Emission and Field Ionization* (Harvard University, Cambridge, MA, 1961).
- <sup>37</sup>Y. Saito, K. Hamaguchi, K. Hata, K. Tohji, A. Kasuya, Y. Nishina, K. Uchida, Y. Tasaka, F. Ikazaki, and M. Yumura, *Ultramicroscopy* **73**(1-4), 1 (1998).
- <sup>38</sup>K. A. Dean, P. von Allmen, and B. R. Chalamala, *J. Vac. Sci. Technol. B* **17**(5), 1959 (1999).
- <sup>39</sup>K. A. Dean, T. P. Burgin, and B. R. Chalamala, *Appl. Phys. Lett.* **79**, 1873 (2001).
- <sup>40</sup>K. Hata, A. Takakura, and Y. Saito, *Surf. Sci.* **490**, 296 (2001).
- <sup>41</sup>C. J. Edgcombe and U. Valdré, *Philos. Mag. B* **82**, 987 (2002).
- <sup>42</sup>S. T. Purcell, P. Vincent, C. Journet, and V. T. Binh, *Phys. Rev. Lett.* **88**, 105502 (2002).
- <sup>43</sup>J.-M. Bonard, C. Klinke, K. A. Dean, and B. F. Coll (unpublished).
- <sup>44</sup>R. T. K. Baker, in *Carbon Fibers, Filaments, and Composites, NATO Advanced Studies Institute, Series E*, Vol. 177 (Plenum, New York, 1990), p. 507.
- <sup>45</sup>R. T. K. Baker, J. R. Alonzo, J. A. Dumesic, and D. J. C. Yates, *J. Catal.* **77**, 74 (1982).

- <sup>46</sup>K. A. Dean and B. R. Chalamala, *Appl. Phys. Lett.* **85**(7), 3832 (1999).
- <sup>47</sup>J.-M. Bonard, N. Weiss, H. Kind, T. Stöckli, L. Forró, K. Kern, and A. Châtelain, *Adv. Mater.* **13**, 184 (2001).
- <sup>48</sup>M. Chhowalla, K. B. K. Teo, C. Ducati, N. L. Rupesinghe, G. A. J. Amaratunga, A. C. Ferrari, D. Roy, J. Robertson, and W. I. Milne, *J. Appl. Phys.* **90**(10), 5308 (2001).
- <sup>49</sup>C. A. Bower, O. Zhou, Z. Wei, D. J. Werder, and J. Sungho, *Appl. Phys. Lett.* **77**(17), 2767 (2000).
- <sup>50</sup>C. Klinke, J.-M. Bonard, and K. Kern, *J. Phys. Chem. B* **106**, 11 191 (2002).
- <sup>51</sup>R. T. K. Baker and R. J. Waite, *J. Catal.* **37**, 101 (1975).
- <sup>52</sup>R. Gao, Z. Pan, and Z. L. Wang, *Appl. Phys. Lett.* **78**, 1757 (2001).
- <sup>53</sup>Y. Zhang, A. Chang, J. Cao, Q. Wang, W. Kim, Y. Li, N. Morris, E. Yenilmez, J. Kong, and H. Dai, *Appl. Phys. Lett.* **79**, 3155 (2001).
- <sup>54</sup>B. F. Coll, K. Dean, Y. Wei, J. Jaskie, and J.-M. Bonard (unpublished).
- <sup>55</sup>C. Bower, Z. Wei, J. Sungho, and O. Zhou, *Appl. Phys. Lett.* **77**(6), 830 (2000).
- <sup>56</sup>Wolfram Research, [www.wolfram.com](http://www.wolfram.com)